COBEM 2021 26th International Congress of Mechanical Engineering
ABCM Associação Brasileira de Engenharia e Ciências Mecânicas
November 22-26, 2021, Virtual Congress, Brazil

COBEM2021-1761
NUMERICAL SIMULATIONS OF MULTIPHASE FLOW WITH COMPRESSIBILITY EFFECTS

Alessandra Ribeiro da Silva
Fluid Mechanics Laboratory, Federal University of Uberlândia, 2121 Av. João Naves de Ávila, Uberlândia, Brazil
alessandra.silva@ufu.br

Rafael Romão da Silva Melo
Department of Thermal Science and Fluids, Federal University of São João del-Rei, 170 Frei Orlando Square, São João del-Rei, Brazil
rafaelmelo@ufsj.edu.br

Aristeu da Silveira Neto
Fluid Mechanics Laboratory, Federal University of Uberlândia, 2121 Av. João Naves de Ávila, Uberlândia, Brazil
aristeus@ufu.br

Abstract. *This present work presents numerical simulations of multiphase flow with compressibility effects. The multiphase flow is modeled with the volume of fluid technic, and the compressibility is modeled using a pressure-based calculation method. All of the simulations were carried out using a computational code that was developed at home (MFSim - Multiphysics Simulator). We perform three validation cases: The shock tube with two gas, compressible water flow over an air bubble, and supersonic flow over a liquid drop. Consistent qualitative results are obtained, and corresponding quantitative results compare well with the analytical solutions and the reference results that other authors have published.*

Keywords: *Compressible flow, Multiphase flow, Adaptive mesh refinement*

1. INTRODUCTION

With the advancement of computational resources, numerical solutions have been used to evaluate industrial applications. In this sense, numerical/computational modeling is a viable alternative to optimize industrial processes. To obtain more accurate results, it is necessary that this modeling consider numerous phenomena that occur during the various process that occurs in the industry.

In these industrial applications, there are regions where the flow is compressible and other areas where fluid compressibility is minimal or non-existent. Thus, it is necessary to study and implement numerical techniques that solve incompressible or compressible flows depending on the flow characteristic. These techniques that encompass all regimes, from incompressible to supersonic, are known as *All-Mach* Techniques, or techniques that solve the flow at any speed (Maliska, 1995).

In industrial processes, the fluid can be in two distinct phases or situations with two or more immiscible fluids. In this case, considering also flows at high Mach numbers, mathematical and numerical modeling is challenging.

Another of the greatest challenges that is found in the area of computational experimentation is the efficiency of computational tools. The use of an adaptive grid is a powerful way to save mesh refinement and, consequently, save processing time. This method of discretizing the equations allows the mesh to adapt dynamically to the physical or geometric requirements of a given problem. For example, a more refined mesh is required near a wall or on a turbulent wake. Several works have been developed employing adaptive mesh, with block-structured mesh (Berger and Colella, 1989; Bell *et al.*, 1994; Berger and LeVeque, 1998; Baeza and Mulet, 2006; George and LeVeque, 2006). This approach was selected to be implemented in the present work.

This present work presents numerical simulations of multi-phase flow with compressibility effects. The multi-phase flow is modeled with the volume of fluid technic, and the compressibility is modeled using a pressure-based calculation method. All the implementations and simulations are carried out using an in-house computational code named MFSim (Multiphysic Simulator), which allows to solve the Navier-Stokes equations in the transient three-dimensional form using block-structured mesh with local adaptability.

2. MATHEMATICAL MODEL

In this section, the partial differential equations that model the problem along with the boundary conditions and initial conditions are presented, when applicable. In all simulated cases, compressible flows of Newtonian fluids are considered. The equation of the mass balance for the case of compressible flow in Cartesian coordinates, using the index notation is given by Eq. (1).

$$\frac{\partial \rho}{\partial t} + \frac{\partial \rho u_j}{\partial x_j} = 0, \quad j = 1, 2, 3, \tag{1}$$

where ρ is the specific mass, t the time variable, u_j is the fluid velocity component in j direction and x_j are the Cartesian coordinates directions x, y and z, respectively. Equation (2) represents the balance of the momentum, written in divergent form, in Cartesian coordinates and in indicial notation.

$$\frac{\partial \rho u_i}{\partial t} + \frac{\partial \rho u_i u_j}{\partial x_j} = -\frac{\partial p}{\partial x_i} + \frac{\partial}{\partial x_j}\left[\mu\left(\frac{\partial u_i}{\partial x_j} + \frac{\partial u_j}{\partial x_i}\right) - \frac{2}{3}\mu\left(\frac{\partial u_k}{\partial x_k}\right)\delta_{i,j}\right], \tag{2}$$

where $i, j = 1, 2, 3$, p is the pressure, t is the time, and δ defined as the Kronecker operator.

Equation (3) represents the thermal energy balance for a Newtonian fluid, written in divergent form, in Cartesian coordinates and in indicial notation.

$$\frac{\partial (\rho c_p T)}{\partial t} + \frac{\partial \left(\rho c_p T u_i\right)}{\partial x_i} = \frac{\partial}{\partial x_i}\left(k\frac{\partial T}{\partial x_i}\right) + \Phi + \lambda \tag{3}$$

where i, j and $k = 1, 2, 3$, c_p is the specific heat at constant pressure and Φ and λ are given by Eqs. (4) and (5), respectively.

$$\Phi = \mu\left[\left(\frac{\partial u_i}{\partial x_j} + \frac{\partial u_j}{\partial x_i}\right)^2 + \left(\frac{\partial u_i}{\partial x_k} + \frac{\partial u_k}{\partial x_i}\right)^2 + \left(\frac{\partial u_j}{\partial x_k} + \frac{\partial u_k}{\partial x_j}\right)^2 + 2\left(\frac{\partial u_i}{\partial x_i}\right)^2\right] - \frac{2}{3}\mu\left(\frac{\partial u_i}{\partial x_i}\right)^2 \tag{4}$$

$$\lambda = \frac{\partial p}{\partial t} + u_i\frac{\partial p}{\partial x_i} \tag{5}$$

In the present work, the SIMPLE (Semi-Implicit Method for Pressure Linked Equations) method developed by Patankar and Spalding (1983) was used in a Cartesian and staggered grid. In this method the equations for the correction of velocities are obtained by from the momentum equations and mass balance equation. For more details, see Ferziger and Peric (2012).

2.1 VOF methodology

The VOF method (Hirt and Nichols, 1981) is one of the oldest methods used in the representation of flows with the presence of an interface between different fluids. Its first applications were made in simulations of free-surface flows. Nowadays, the literature available in the scientific community presents several types of application of the method, such as in bubble, droplet, and other types of fluid interfaces.

In the VOF method, the α function is responsible for defining where the different types of fluid are located in the domain and the interface(s) that separate them. For example, in a gas/liquid system described in a Cartesian mesh, the function α assumes a unit value for the volumes that contain the liquid phase and zero for the gas phase. The interface between the phases is described through volumes that store intermediate values of the α function, representing a volumetric fraction of a specific phase contained in the volume in question. The function α is advected from the flow velocity field through the Eq. 6.

$$\frac{\partial \alpha}{\partial t} + (u \cdot \nabla)\,\alpha = 0 \tag{6}$$

The Laplace equation (Eq. 7) gives the pressure jump in the interface:

$$p_{II} - p_I = \sigma\kappa \tag{7}$$

The calculation of the interfacial force used in the simulations was proposed by Brackbill *et al.* (1992), the CSF (Continuum Surface Force). In this method, the interfacial force per unit area is calculated on the face $(i-1/2, j, k)$ using the Eq.8:

$$f_{\sigma_{i-1/2,j,k}} = \sigma \cdot \kappa_{i-1/2,j,k} \cdot \alpha^*_{i-1/2,j,k}, \tag{8}$$

where $\alpha^*_{i-1/2,j,k} = \dfrac{\alpha_{i,j,k} - \alpha_{i-1,j,k}}{\Delta x}$ and the curvature is interpolated from the center of neighboring cells using a weighted average.

2.2 *All-Mach* methodology

Few numerical methods apply to both incompressible and compressible flows. The scientific community's effort to seek general ways to solve flows for any Mach number began in the late 1960s. Pioneering work in this line was by the authors Harlow and Amsden (1968) who proposed a technique, called ICE, to the solution of transient problems contemplating an extensive range of the Mach number.

More recently, Darwish (2000) have reformulated the SIMPLE's family using a co-located mesh approach to predict single fluid flows at any Mach number. Furthermore, the philosophies behind these algorithms, as well as their similarities and differences, are explained. Later, Darwish and Moukalled (2014) extended these reformulations, mentioned above, to the case of flows with more than one fluid. Darwish *et al.* (2007, 2009) also presented a fully coupled method for incompressible flows and in a recent work Darwish and Moukalled (2014) extended this fully coupled algorithm to situations involving compressible flows.

The main idea for creating an *All-mach* solver is the deduction of an equation for the pressure fluctuation that takes into account the density variation due to the fluid's compressibility. For this, we started from the equation of complete continuity and linearized the specific mass-velocity product as follows:

$$\rho u_i = \rho' {u_i}^* + \rho^* {u_i}' - \rho^* {u_i}^*, \tag{9}$$

where ρ^* and ${u_i}^*$ are the specific mass and estimated velocities in this iteration (Maliska, 1995)

The term u_i' brings the contribution of the pressure fluctuation of the *momentum* equation:

$${u_i}' = {u_i}^* - \frac{1}{A_{pU_i}} \frac{\partial p'}{\partial x_i}. \tag{10}$$

And the term ρ' brings the contribution of density variation due to pressure variation (fluctuation), which the equation of state can model:

$$\rho' = \frac{p'}{RT}, \tag{11}$$

where p' is the pressure fluctuation, R is the universal gas constant, and T is the fluid temperature.

Combining the Eqs. 9, 10 and 11 with the continuity equation for a compressible fluid (Eq. 1), we obtain an equation for the pressure fluctuation that operates in the most distinct Mach numbers, being able to simulate incompressible, subsonic, transonic, and even supersonic flows (Ferziger and Peric, 2012; Maliska, 1995).

2.3 Coupling of *All-Mach* and VoF methodologies

When dealing with multiphase flows, it is necessary to treat the specific mass for each phase, being, for example, a gas phase and a liquid phase. Several authors propose using an equation of general state valid for any fluid, such as air or even water. For some applications, the hypothesis that liquids are incompressible is reasonable. Still, this hypothesis may not be accepted for other applications, such as flows at high pressures, since compressibility effects may occur in this liquid.

In this context, we modeled and implemented a general equation of state in the MFSim code in such a way as to model any compressible flow, without the need to check whether the fluid (or one of the fluid phases if the flow is two-phase) meets the hypothesis or not compressibility.

As shown earlier, the *All-Mach* technique uses the ideal gas equation in the pressure fluctuation equation so that the solver takes into account the variation in specific mass due to variations in pressure and temperature. To deduce the pressure fluctuation equation to the new general state equation, we must carry out the same procedure. The general state equation is as follows:

$$\rho = \frac{p + p_\infty}{\left(\frac{\gamma-1}{\gamma} C_p\right) T}, \tag{12}$$

where ρ is the specific mass, p is the pressure, γ is the coefficient of adiabatic expansion, C_p is the specific heat at constant pressure, T is the temperature, and $p\ infty$ is a auxiliary variable. If $p_\infty = 0$ the general state equation reduces to the ideal gas equation, and if $p_\infty \neq 0$ this equation is used to model other fluids, for example water.

Next, the deduction of an equation for the specific mass will be presented, which will be used in the pressure fluctuation equation. To calculate the specific mass in the current iteration $n+1$ we use the pressure at the same time:

$$\rho^{n+1} = \frac{p^{n+1} + p_\infty}{\left(\frac{\gamma-1}{\gamma} C_p\right) T}. \tag{13}$$

However, as the system of equations is non-linear, then we need to use estimates. To calculate the estimated specific mass ρ^* we use the estimated pressure p^* from the previous iteration:

$$\rho^* = \frac{p^* + p_\infty}{\left(\frac{\gamma-1}{\gamma} C_p\right) T}. \tag{14}$$

Subtracting the Eq. (14) from the Eq. (13) we obtain:

$$\rho^{n+1} = \rho^* + \frac{p^{n+1} - p^*}{\left(\frac{\gamma-1}{\gamma} C_p\right) T}. \tag{15}$$

The pressure difference over time is the pressure fluctuation p'. Thus:

$$\rho = \rho^* + \frac{p'}{\left(\frac{\gamma-1}{\gamma} C_p\right) T}. \tag{16}$$

This equation for specific mass is identical to the one found for the ideal gases above. So the algorithm of the pressure fluctuation solution remains the same for the new general state equation. In the code, the only difference between using this equation or simply using the ideal gas equation is in calculating the estimated specific mass, since this general equation has a new constant, p_∞.

3. RESULTS AND DISCUSSION

3.1 Two gas shock tube

The problem of the shock tube with two perfect gases is performed. The initial condition is presented in Figure 1. This solution will validate the All-Mach technique coupled with a multiphase flow solution, using the VoF methodology as presented above. Initially there is an interface located at $x = 0.5$ m, separating the two perfect gases with different specific heat ratios ($\gamma = c_p/c_v$). The two fluids are initially with null velocity, and there is a jump in specific mass, pressure, and γ.

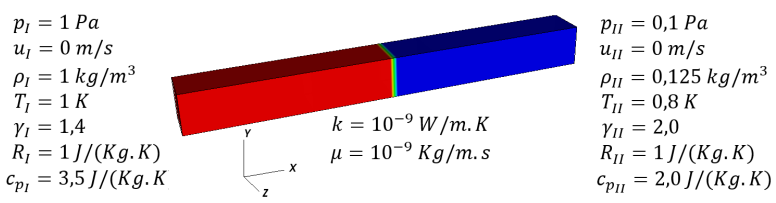

Figure 1. Physical properties of the two gases.

In Table 1 we have the necessary information for the computational simulation.

Figure 2 shows the density field in color and the interface between the two fluids represented by the black line. Position X_1 is the expansion wave front, which moves to the left, region X_3 is the shock wave, and region X_2 is the region where

Table 1. Data from the simulation of the two gas case

Computational setup	
Domain	$1[m] \times 0.08[m] \times 0.08[m]$
Mesh	$200 \times 8 \times 8$
Time discretization scheme	EULER
Advective scheme	SUPERBEE
CFL	0.1
Final simulation time	$0.2s$
Boundary condition on input	Dirichilet for u,v,w,p,T
Boundary condition in output	Dirichilet for u,v,w,p,T
Boundary condition for other faces	Symmetry

Figure 2. Specific mass field and interface between the two fluids (black line).

the two initial fluids separate, regardless of whether the initial fluid pair is monophasic or biphasic. Note that the *VoF* interface follows this region that delimits the fluids, showing that it was well advected.

In Fig. 3 the pressure profiles, specific mass, and longitudinal component of velocity (u) are presented. The simulations carried out with the SUPERBEE scheme demonstrated behavior consistent with the analytical solution. Still, there is a slight increase in the value in the velocity profile between $x = 0.65$ m and $x = 0.85$ m approximately. To solve this problem, we will perform simulations with other TVD's schemes, and we will also make simulations with a finer mesh.

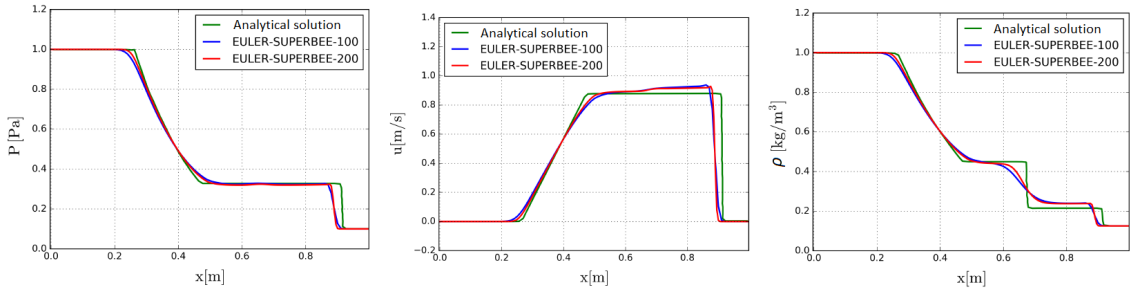

Figure 3. Pressure profiles, specific mass and u component of velocity.

3.2 Compressible water flow over an air bubble

In this section, the results of compressible water flow over a gas bubble will be presented. In the VOF methodology, the continuous phase was filled with water, and we use the equation of state for a liquid to calculate the specific mass, while the dispersed phase was used to represent air, in which case the equation of state for an ideal gas.

The Table 2 shows the details of the computational setup:

Table 2. Data from the simulation of the case

Computational setup	
Domain	$0.024[m] \times 0.006[m] \times 0.00024[m]$
Initial diameter of the bubble	$D = 0,006[m]$
Mesh	$1780 \times 356 \times 4$
Time discretization scheme	EULER
Advective scheme	SUPERBEE
CFL	0.2
Final simulation time	$t_1 = 3,8x10^{-6}$

The values used in the initial conditions for speed, pressure, temperature and fluid properties are shown in Fig. (4).

The Figure (5) presents the temporal evolution of the flow in the present case. The results are in good agreement with

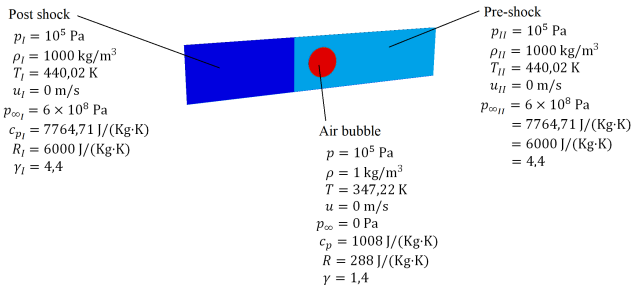

Figure 4. Initial condition - water flow over the air bubble

the data extracted from the reference Majidi and Afshari (2015). It is observed that when the wave collides with the air bubble, it deforms with the injection of water along the centerline. Note the deformation in the concave shape, as in the reference.

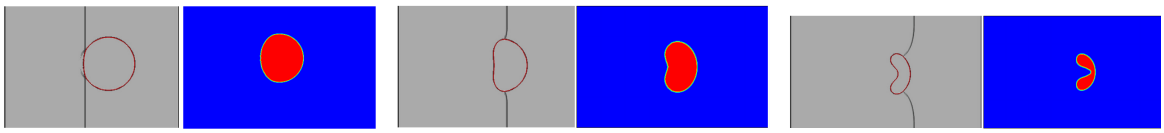

(a) Instant 1 (b) Instant 2 (c) Instant 3

Figure 5. Temporal evolution of the flow.

3.3 Supersonic flow over a liquid drop

As a step in validating the algorithm in a supersonic flow, we performed the simulation of the supersonic airflow over an immersed liquid drop. The numerical experiment was performed based on the work of Xiao *et al.* (2016). The diameter of the drop is equal to $0.1\ mm$. The density and viscosity of the liquid are, respectively, $\rho_l = 978\ kg/m^3$ and $\mu_l = 0.6667\ 10^{-3}\ Pa \cdot s$. The temperature and pressure of the free current are $T_\infty = 107\ K$ of $P_\infty = 1620\ Pa$, with low density air of $\rho_\infty = 0.05274\ kg/m^3$. The velocity of the free current U_∞ is 622 m/s, and the resulting Mach number is $Ma = 3$. The viscosity of the free current used is $\mu_L = 0.743\ 10^{-5}\ Pa$, resulting in the Reynolds number $Re = 441.5$. The coefficient of surface tension between the fluid pair is $\sigma = 0.0273\ N/m$.

The computational domain is $[0.10D] \times [0.4D] \times [0.4D]$, in the directions x, y and z, respectively. The center of the initial static drop is located at the position $(2D, 2D, 2D)$.

To verify the functionality of the MFSim code in stages, first a two-dimensional simulation was performed, using a domain with dimensions $[0.10D] \times [0.4D]$, and the drop is represents like a cylinder. Figure 6 shows the initial velocity field and the drop positioned at $(2D, 2D)$. A base mesh of $80 \times 32 \times 1$ volumes was used, a level of refinement initially applied to the input and contouring the drop. The adaptive mesh was used throughout the simulation, and the refinement criteria used were density gradient and vorticity magnitude.

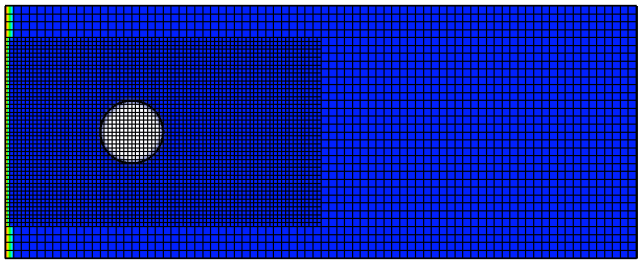

Figure 6. Initial velocity field for the two-dimensional case.

Figure 7 shows the evolution of the flow over time for this initial two-dimensional test. Note the formation of a shock wave at the domain entrance, and with the advance of time, this shock wave reaches the water drop. The refinement follows the density gradient, which is more expressive in the contact between the two phases, and in the region with great vorticity.

As good numerical stability and convergence of variables in the MFSim were observed for the two-dimensional case, we performed the simulation of the three-dimensional case. Fig. 8 presents the initial velocity field and the drop positioned immersed in the air.

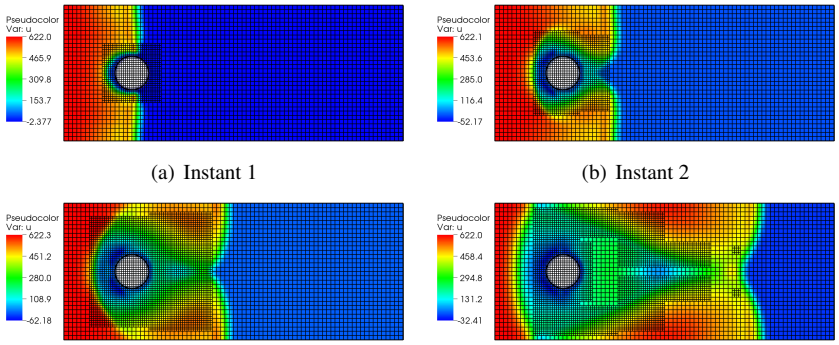

(a) Instant 1 (b) Instant 2

(c) Instant 3 (d) Instant 4

Figure 7. Temporal evolution for the two-dimensional case.

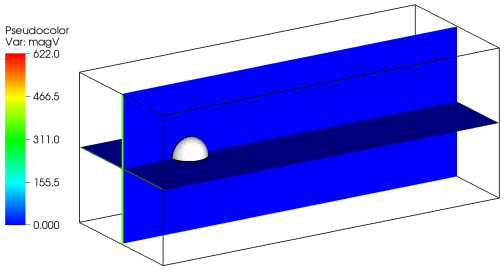

Figure 8. Initial velocity field for the three-dimensional case.

Figure 9 shows the evolution of the flow over time for the three-dimensional case. Similar to what happened in the case in two dimensions, a shock wave is formed at the domain entrance, which propagates in the flow direction, reaches the static drop, and then the fluid surrounds this drop and occurs the formation of a wake downstream of the drop water.

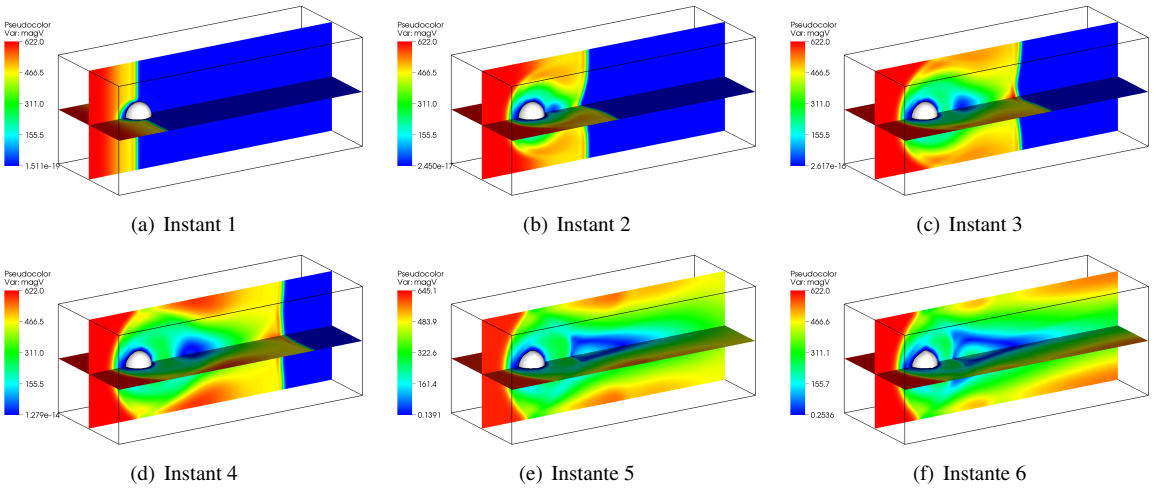

(a) Instant 1 (b) Instant 2 (c) Instant 3

(d) Instant 4 (e) Instante 5 (f) Instante 6

Figure 9. Temporal evolution for the three-dimensional case.

Figure 10 shows the deformed droplet at the simulated final instant. Note that it assumes a conical shape due to supersonic flow. It is also possible to observe that the *VoF* methodology remained stable, showing no numerical oscillation, thus being an efficient way to model two-phase flows using the *All-mach* technique developed in the context of this work.

Figure 11 shows the position of the shock wave that forms on the drop in dimensionless time $t^* = 0.04$ in a central plane $Z = 2D$. Note the formation of a shock wave over the drop, similar to the result presented by Xiao *et al.* (2016).

4. CONCLUSION

This present work presents numerical simulations of multi-phase flow with compressibility effects. The multi-phase flow is modeled with the volume of fluid technic, and the compressibility is modeled using a pressure-based calculation method. All the implementations and simulations are carried out using an in-house computational code named MFSim (Multiphysic Simulator) Satisfactory results were obtained for the benchmark test cases, showing a good efficiency of the

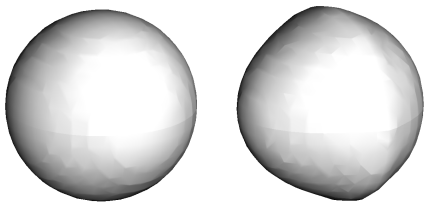

(a) Initial time (b) Final time

Figure 10. Drop deformation due to flow.

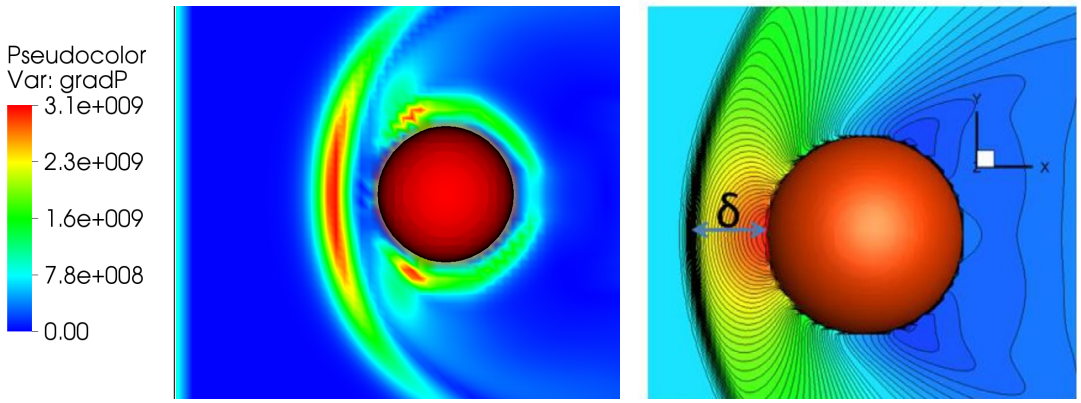

(a) Presente (b) Xiao *et al.* (2016)

Figure 11. Comparison of the shock wave over drop in time $t^* = 0.04$.

applied technique. To reduce the computational cost, the adaptive mesh technique was used, refining only in the region of interest.

5. ACKNOWLEDGEMENTS

The authors gratefully acknowledge financial support from PETROBRAS, CEFET-MG, Capes, CNPQ and Fapemig. The authors are also grateful to the mechanical engineering graduate program from the Federal University of Uberlândia (UFU).

6. REFERENCES

Baeza, A. and Mulet, P., 2006. "Adaptive mesh refinement techniques for high-order shock capturing schemes for multi-dimensional hydrodynamic simulations". *International Journal for Numerical Methods in Fluids*, Vol. 52, No. 4, pp. 455–471. doi:10.1002/fld.1191.

Bell, J., Berger, M., Saltzman, J. and Welcome, M., 1994. "Three-dimensional adaptive mesh refinement for hyperbolic conservation laws". *SIAM Journal on Scientific Computing*, Vol. 15, No. 1, pp. 127–138. doi:10.1137/0915008.

Berger, M. and LeVeque, R., 1998. "Adaptive mesh refinement using wave-propagation algorithms for hyperbolic systems". *SIAM Journal on Numerical Analysis*, Vol. 35, No. 6, pp. 2298–2316. doi:10.1137/S0036142997315974.

Berger, M. and Colella, P., 1989. "Local adaptive mesh refinement for shock hydrodynamics". *Journal of Computational Physics*, Vol. 82, No. 1, pp. 64 – 84. ISSN 0021-9991. doi:10.1016/0021-9991(89)90035-1.

Brackbill, J.U., Kothe, D.B. and Zemach, C., 1992. "A continuum method for modeling surface tension". *Journal of computational physics*, Vol. 100, No. 2, pp. 335–354.

Darwish, M. and Moukalled, F., 2014. "A fully coupled navier-stokes solver for fluid flow at all speeds". *Numerical Heat Transfer, Part B: Fundamentals*, Vol. 65, No. 5, pp. 410–444.

Darwish, M., Sraj, I. and Moukalled, F., 2007. "A coupled incompressible flow solver on structured grids". *Numerical Heat Transfer, Part B: Fundamentals*, Vol. 52, No. 4, pp. 353–371.

Darwish, F Moukalled, M., 2000. "A unified formulation of the segregated class of algorithms for fluid flow at all speeds". *Numerical Heat Transfer: Part B: Fundamentals*, Vol. 37, No. 1, pp. 103–139.

Darwish, M., Sraj, I. and Moukalled, F., 2009. "A coupled finite volume solver for the solution of incompressible flows on unstructured grids". *Journal of Computational Physics*, Vol. 228, No. 1, pp. 180–201.

Ferziger, J.H. and Peric, M., 2012. *Computational methods for fluid dynamics*. Springer Science & Business Media.

George, D. and LeVeque, R., 2006. "Finite volume methods and adaptive refinement for global tsunami propagation and local inundation". *Science of Tsunami Hazards*, Vol. 24, No. 5, pp. 319–328.

Harlow, F.H. and Amsden, A.A., 1968. "Numerical calculation of almost incompressible flow". *Journal of Computational Physics*, Vol. 3, No. 1, pp. 80–93.

Hirt, C.W. and Nichols, B.D., 1981. "Volume of fluid (vof) method for the dynamics of free boundaries". *Journal of computational physics*, Vol. 39, No. 1, pp. 201–225.

Majidi, S. and Afshari, A., 2015. "Towards numerical simulations of supersonic liquid jets using ghost fluid method". *International Journal of Heat and Fluid Flow*, Vol. 53, pp. 98–112.

Maliska, C., 1995. *Transferência de Calor e Mecânica dos Fluídos Computacional*. LTC.

Patankar, S.V. and Spalding, D.B., 1983. "A calculation procedure for heat, mass and momentum transfer in three-dimensional parabolic flows". In *Numerical Prediction of Flow, Heat Transfer, Turbulence and Combustion*, Elsevier, pp. 54–73.

Xiao, F., Wang, Z., Sun, M., Liang, J. and Liu, N., 2016. "Large eddy simulation of liquid jet primary breakup in supersonic air crossflow". *International Journal of Multiphase Flow*, Vol. 87, pp. 229–240. ISSN 0301-9322. doi:https://doi.org/10.1016/j.ijmultiphaseflow.2016.08.008. URL `http://www.sciencedirect.com/science/article/pii/S0301932215300744`.

7. RESPONSIBILITY NOTICE

The authors are solely responsible for the printed material included in this paper.